THE EUROPEAN
PHYSICAL JOURNAL D

Regular Article

Low energy electron transport in furfural[★]

Ana I. Lozano[1], Kateryna Krupa[1,2], Filipe Ferreira da Silva[2], Paulo Limão-Vieira[2], Francisco Blanco[3], Antonio Muñoz[4], Darryl B. Jones[5], Michael J. Brunger[5], and Gustavo García[1,a]

[1] Instituto de Física Fundamental, Consejo Superior de Investigaciones Científicas, Serrano 113-bis, 28006 Madrid, Spain
[2] Laboratório de Colisões Atómicas e Moleculares, CEFITEC, Departamento de Física, Faculdade de Ciências e Tecnologia, Universidade NOVA de Lisboa, 2829-516 Caparica, Portugal
[3] Facultad de Ciencias Físicas, Universidad Complutense de Madrid, 28040 Madrid, Spain
[4] Centro de Investigaciones Energéticas, Medioambientales y Tecnológicas, Avenida Complutense 22, 28040 Madrid, Spain
[5] School of Chemical and Physical Sciences, Flinders University, GPO Box 2100, Adelaide, SA 5001, Australia

Abstract. We report on an initial investigation into the transport of electrons through a gas cell containing 1 mTorr of gaseous furfural. Results from our Monte Carlo simulation are implicitly checked against those from a corresponding electron transmission measurement. To enable this simulation a self-consistent cross section data base was constructed. This data base is benchmarked through new total cross section measurements which are also described here. In addition, again to facilitate the simulation, our preferred energy loss distribution function is presented and discussed.

1 Introduction

In the last few years we have paid considerable attention, in collaboration with other international research groups, to the study of electron interactions with furfural molecules (see Refs. [1–4] and references therein). Furfural is a relevant molecule for the combustion industries, as a potential fuel derived from atmospheric-plasma treatments of biomass [5–8]. In addition, its cyclic molecular configuration (see Fig. 1) is similar to the 5-membered ring structure constituting the sugar units of the DNA helix. Previous theoretical and experimental studies focused on electron interaction processes such as differential (DCS) and integral (ICS) elastic scattering cross sections [1], vibrational and electronic excitation by electron and photon impact [2–4,9,10], and integral inelastic, ionisation [1] and total scattering cross sections (TCS) [1]. Very recently, direct total scattering cross sections have been measured with a double spectrometer transmission beam system [11]. Further to these studies, a comprehensive data set of electron scattering cross sections over a broad energy range, from 0.1 to 10 000 eV, is now available for modelling purposes. However, an important feature of these databases is their reliability in terms of agreement between theory and experiment, consistency between differential, integral and total scattering data and their estimated uncertainty limits. Thus one of the main goals of

this study is to contribute to the evaluation of low energy electron scattering cross sections from furfural, by providing new measurements of the total scattering cross sections for selected energies (7, 10 and 20 eV) using a magnetically confined electron transmission experiment [12,13] developed and implemented in the Madrid laboratory. In addition, energy loss distribution functions for these electron impact energies have also been determined in an angular and energy resolved crossed beam experiment. These have subsequently been combined with our previous differential and integral cross section calculation results and then used as input parameters for an event-by-event Monte Carlo code to simulate the transport of 10 million electrons with an initial energy of 10 eV, through gaseous furfural when the electron beam is confined by an intense axial magnetic field. By comparing the simulated energy distribution of the transmitted electrons with the experimental observation, the reliability of the scattering cross sections as well as the relevance of multiscattering processes has been analysed.

This paper is divided in five sections. Following the introduction, the experimental techniques used to determine the total scattering cross sections, the energy loss distribution functions and the energy distribution of the transmitted electrons are described in Section 2. Section 3 includes a brief description of the calculation method used to determine the elastic DCS and elastic and inelastic ICS for furfural, and some details of the Monte Carlo simulation procedure used to model the electron transport. Our experimental and theoretical results are presented and discussed in Section 4, together with a comparison between
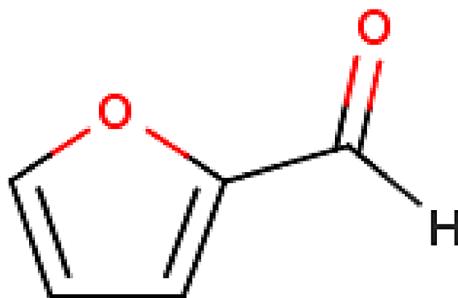
Fig. 1. Schematic representation of the cis-isomer structure of furfural.

the observed and simulated energy distributions after the electron transport process. Finally, we draw some conclusions from this study in Section 5.

2 Total cross section measurements

The present experimental configuration is based on a previously described apparatus [12,13], with a schematic representation being shown in Figure 2. Briefly, the apparatus consists of an electron beam generated by an emitting filament, which is axially confined by a magnetic field (B_1) and then collimated and accelerated through the entrance aperture of the scattering chamber. The scattering chamber (SC) is a 240 mm length cylinder, whose entrance and exit apertures are defined by two 2 mm diameter and 5 mm thickness apertures. Another axial magnetic field (B_2) is applied to the scattering cell, which is generated by an independent coil. Electrons transmitted through SC enter the analyser region, where a third axial magnetic field (B_3) is provided by a further pair of solenoids. The primary electron beam is generated by a hairpin thorium-tungsten filament, which provides direct electron currents in the range of 10^{-8}–10^{-9} A. The electron gun is negatively biased with a variable 0–500 V power supply, which defines its kinetic energy. A three collimator system is used to pulse the electron beam, typically with 0–500 V negative pulses and with a time duration of 10 ms and 100 Hz repetition rate. Electrons passing through the SC are analysed in energy with a retarding field analyser (RFA), which consists of three 2 mm diameter collimators. The two external electrodes of the RFA are grounded, while the central one is connected to an adjustable 0–500 V negative power supply. The system is differentially pumped by means of two 300 l·s^{-1} turbo pumps which are connected to the electron gun and RFA regions, respectively. The background pressure in the gun and RFA regions was typically 10^{-8} Torr, and it was always maintained lower than 10^{-7} Torr even during measurements when the furfural pressure in the scattering chamber reached values up to 1.2 mTorr. Electrons transmitted through the RFA are finally detected by a two-step microchannel plate (MCP) system operating in single pulse count mode. The collected charge is converted into single voltage pulses by means of a charge sensitive preamplifier, while standard "EG&G Ortec" amplifier-discriminator provided TTL pulses ready to be stored and analysed on a personal computer. Fi-

nally we note that the RFA voltage, the electron pulsing and the electron counter systems are controlled by a National Instrument data acquisition card operating under a LabView environment.

As described in references [12,13], the main effect of B_2 (typically ∼0.05 T) is to compensate for the perpendicular component of the velocity of the scattered electrons and so it converts a potential deflection into a velocity loss along the axial component. In these conditions, elastic electron scattering processes can be quantified by analysing the subsequent kinetic energy loss of transmitted electrons. If an inelastic process takes place, an additional energy loss due to the target excitation is also detected by the RFA. Consequently, the energy resolution of the entire system also relates to its angular resolution. The B_1 and B_3 field strengths are varied from 0 to 0.02 T during the measurements, in order to guide the electron beam in the gun and analyser regions, respectively. Figure 3 shows a typical transmitted spectrum for 10 eV incident electrons passing through the scattering chamber in the absence of any furfural. The derivative of this energy distribution is also shown, in order to indicate the typical energy resolution employed in this study (typically 310 meV full width at half maximum).

The total cross sections (TCS), represented by σ_{tot}, are measured by recording the attenuation of the beam intensity as a function of the molecular density, obeying the well-known Beer-Lambert law:

$$I = I_0 \exp(-nL\sigma_{tot}), \tag{1}$$

where I_0 is the intensity of the primary electron beam, I is the transmitted intensity, n is the molecular density and L is the length of the collision chamber ($L = 240$ mm in this case). The molecular density is derived from direct measurements of the pressure (P) and temperature (T) in the gas cell, by assuming an ideal gas behaviour. We can consider this approximation to be valid for the low gas pressures used in this study (0–1.2 mTorr). These measurements were performed with a MKS Baratron 627B capacitance manometer and a standard K-type thermocouple probe, respectively.

The procedure to derive the TCS values from the attenuation measurements is as follows. The operating point (see Fig. 3) is determined by biasing negatively the RFA in order to reduce the transmitted intensity by more than a factor of 2. Using this procedure, the effective energy resolution is substantially improved. Once its operating point is fixed, the transmitted intensity is recorded as a function of pressure over a range for which it decreases by a factor of 10. Typical attenuation curves for 7, 10 and 20 eV incident electron energies are shown in Figure 4, for furfural pressures ranging from 0.2 to ∼1 mTorr.

According to equation (1), the slope (m) of the semi-logarithmic plots shown in Figure 4 ($m = nL$), together with the previously noted pressure and temperature measurements, provide directly the σ_{tot} values. At least five attenuation measurements have been performed for each considered energy, in order to obtain statistical uncertainties within 5–8%. Reproducibility of these types
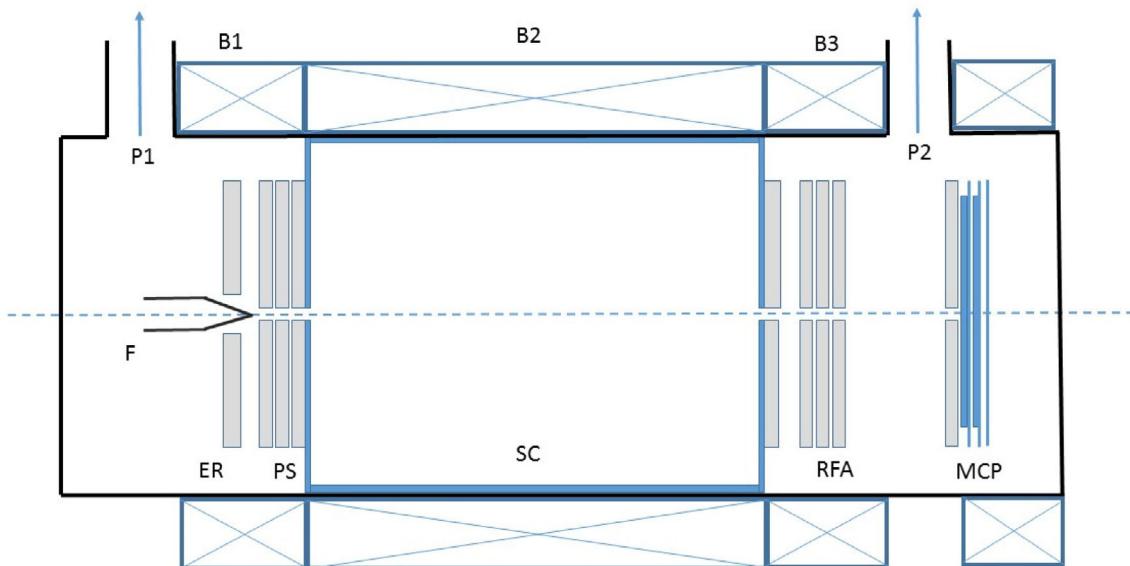
Fig. 2. Schematic diagram of the present experimental setup. B1, B2, B3, coils generating the axial magnetic fields applied to the electron gun, scattering chamber and energy analyser regions, respectively; F is the emitting hairpin filament; PS is the pulsed electrode system; SC, the scattering chamber; RFA represents the retarding field analyser; MCP, the microchannel plate detector and P1, P2 are the turbo pumps.
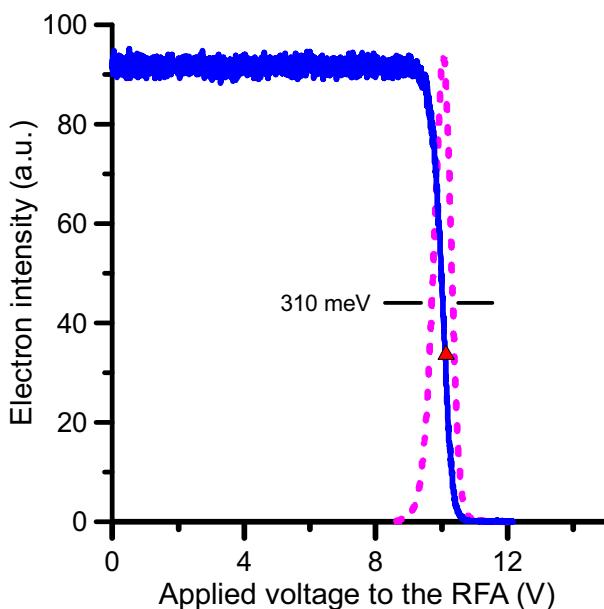

Fig. 3. A typical energy distribution for 10 eV incident electrons transmitted through the retarding field analyser (RFA) (——) and its derivative (- - -). Note that ▲, denotes the operating point.

Fig. 4. Electron attenuation as a function of the furfural pressure for incident energies of 7 eV (▲), 10 eV (▼) and 20 eV (■).

of measurements is typically below 2%, but furfural is a challenging target. Even at low pressures affects the emissivity of the filament, and its "sticky" behaviour affects the accuracy in measuring the SC gas pressure. These problems have been minimized, as much as possible, by working at very low SC pressures and by heating the scattering chamber up to 315–325 K during the measurements. Note that the intrinsic accuracy of pressure mea-
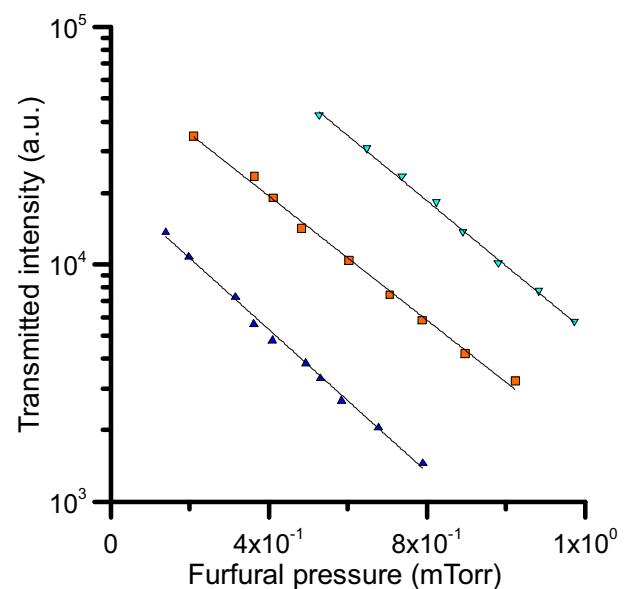
surements has been considered to be within 1%, as stated by the manufacturer of the capacitance manometer (MKS Baratron 627B). In ideal experimental conditions, the axial magnetic field of the scattering chamber is parallel to the velocity vector of incident electrons and therefore no cyclotron deviation should be observed. In practice, the small divergence of the electron beam can generate a cyclotron motion to the incident electrons. However, in the conditions of this experiment we can consider the induced cyclotron radius is almost zero as compared with the geometrical length and aperture diameters of the scattering
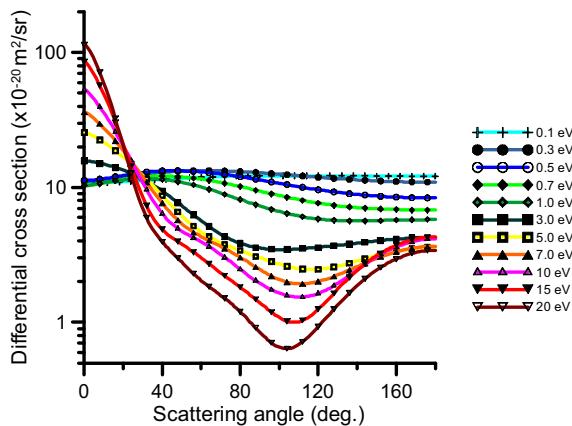
Fig. 5. Elastic differential cross sections for electron scattering from furfural, for incident electron energies from 0.1 to 20 eV. These results are obtained from IAM-SCAR+I [1] computations.

Fig. 6. Integral cross sections calculated with the IAM-SCAR+I procedure, for all considered elastic and inelastic channels (see legend on the plot). Vibrational excitations (●) are taken from reference [3]. Experimental TCS data are shown uncorrected and corrected for missing angles (MA-see text for details). Note that the acronym NR = no rotation, and refers to the IAM-SCAR+I TCS results when rotational excitations are not included.

chamber and therefore we are assuming that the actual scattering length is the geometrical length of the scattering chamber (L). In order to check this assumption, and that other systematic errors such as space charge and multiple scattering effects are not affecting the present results, prior measurements with molecular nitrogen have been performed in the energy range 5–20 eV. Our results for N_2 were found to be in agreement with the recommended values of Itikawa [14] to within 5%. By combining all the known error sources and statistical uncertainties, we obtained total uncertainty limits within 6–9% for the present σ_{tot} for furfural.

3 Modelling procedure

Single electron tracks through the scattering chamber have been simulated with our Low Energy Particle Track Simulation (LEPTS) code [15]. Basically, this is an event-by-event Monte Carlo (MC) simulation procedure which uses the present set of cross section data and experimental energy loss distribution functions as the input parameters. In this case we have extensively utilized the results of our independent atom model with screening corrected additive rule plus interference terms (IAM-SCAR+I) calculation (see Refs. [1,16] and references therein). Differential elastic cross sections have also been calculated using this approach [16], with the angular distribution functions for elastic processes being shown in Figure 5. For the inelastic processes, these angular distribution functions have been modified, in order to account for the excitation energy, according to the procedure described in reference [15].

Integral elastic, electronic excitation and ionization cross sections have been also derived from the IAM-SCAR+I calculation [1]. This approach does not consider nuclear movements, so the vibrational excitation cross sections have been taken from our previous measurements [3]. As described in reference [1], additional rotational excitations have been calculated in the framework of the Born
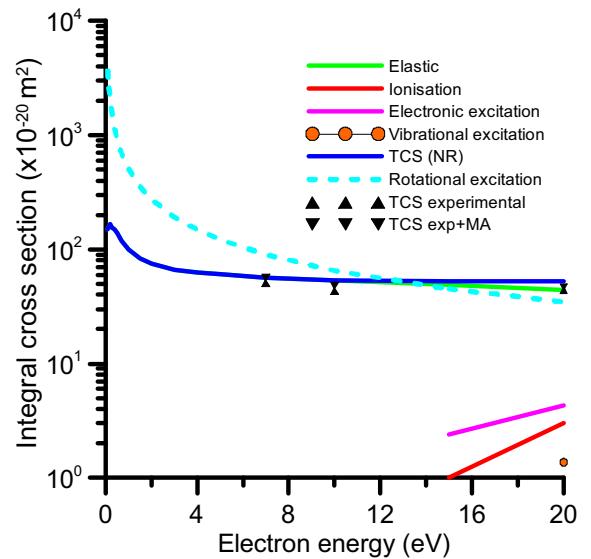
approximation. Note that the rotational excitation energies of furfural are much lower than 300 meV, and therefore collisions inducing rotations are not resolved by our experimental system. Nonetheless, the rotational excitation cross sections published in reference [1] have been also included in the simulation procedure. The integral cross section data used for the transport simulation are listed in Table 1 and plotted in Figure 6.

The current energy loss distribution function has been experimentally determined from the measured energy loss spectra using the crossed-beam technique, as described in references [2,4]. The averaged distribution functions used in this study to determine the energy transferred in inelastic collisions (vibrational excitation, electronic excitation and ionization) during the simulation is shown in Figure 7. This plot corresponds to 10 eV incident electron energies. Once the type of process is sampled by the MC procedure according to the integral cross section probabilities, the energy loss is then sampled by using the distribution function corresponding to that process. In addition, the energy transferred via elastic collisions has been calculated from the corresponding momentum transfer and a constant 10 meV energy transfer, has been assumed for the case of rotational excitations.

Concerning the inclusion of the magnetic field in the simulation, we simply assumed that it was uniform and intense enough to compensate for the perpendicular component of the velocity vector of the colliding electrons. This means that, in a scattering event, no deflection is considered, rather just the energy loss due to the decrement of the parallel component of the velocity vector.

Table 1. The integral electron scattering cross sections ($\times 10^{-20}$ m^2) used as input parameters for our electron transport modelling procedure.

Energy (eV)	Elastic	Ionisation	Electronic excitation	Vibrational excitation	TCS (NR)*	Rotational excitation
1	100				100	510
1.5	83.2				83.2	356
2	74.5				74.5	275
3	66.6				66.6	192
4	62.7				62.7	149
5	60.2				60.2	121
7	56.8		4×10^{-6}		56.8	89.9
10	53.8		0.125		53.9	65.0
15	49.3	1	2.4		52.7	45.1
20	43.7	3	4.34	1.366	52.4	34.7

* Denotes the calculated total cross sections without including rotational excitations.
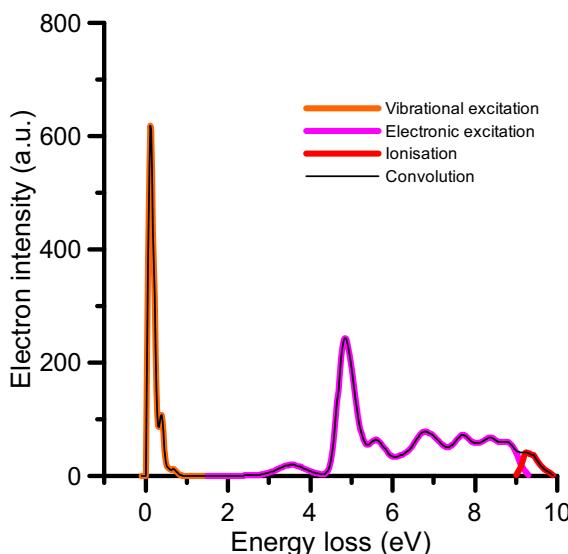

Fig. 7. The present energy loss distribution function as derived from the available experimental spectra [2,4].

Finally, the electron transport behavior has been simulated in this study for 10^7 electrons of 10 eV initial energy, assuming the initial energy distribution shown in Figure 3, and for 1 mTorr of furfural in the scattering chamber. The number of incident electrons has been gradually increased to obtain statistical uncertainties linked to the simulation within 1%, which is about one order of magnitude less than the total uncertainties associated to the cross sections, so there is no effect on the accuracy of the results.

4 Results and discussion

The cross sections determined using the apparatus and measurement procedures described previously, are shown in Table 2, together with their estimated uncertainties for the 7, 10 and 20 eV selected electron energies.
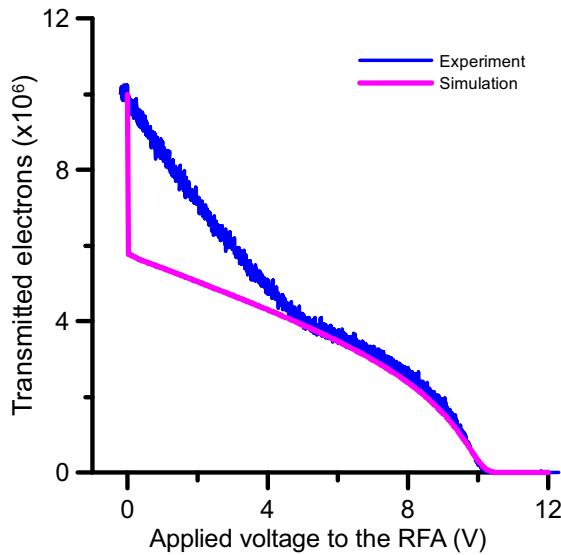
These values were also plotted in Figure 6, so as to compare with the corresponding IAM-SCAR+I calculated data used in the simulation. Due to our energy resolution limitations, the experimental TCS should actually be

compared with the calculated TCS (NR) total cross section, i.e. for the theoretical TCS not including rotational excitations. As can be seen in this figure, the experimental values tend to be lower than the calculated ones by about 20%. However, as mentioned above, the energy resolution limitations lead to missing angles in the forward and backward directions which tends to lower the measured cross sections [12,13]. This follows as electrons elastically scattered into these missing angles are considered by the RFA-detector system as "unscattered" electrons, and therefore the "apparent" total cross section is lower than the actual value. The missing angle magnitudes are shown in the last column of Table 2. The contribution of these missing angles (MA) to the measured TCS value can be estimated by integrating the calculated differential elastic cross sections (see Fig. 5) over those angles. Adding the result of this integration to the measured TCS, we can obtain some "corrected" experimental values (denoted as TCS exp+MA). These values are also plotted in Figure 6 and, as may be seen in this figure, the corrected values are still a little lower than the calculated results by about 10% at worst. This discrepancy is within the estimated uncertainty limits. However, being a systematic behaviour not detected with other targets, such as molecular nitrogen, it seems that the "stickiness" of furfural could affect our measurement of the pressure in the gas cell. In addition this discrepancy is not more significant for 7 eV than for the other energies considered, which indicates that even at that low energy the IAM-SCAR+I procedure cross sections used for the simulation still applies.

The simulated energy distribution for transmitted electrons through the collision chamber, containing 1 mTorr of furfural, is shown in Figure 8. The corresponding transmitted energy distribution, measured with the current experimental system (shown in Fig. 2), is also plotted in this figure for comparison. In both cases, the energy distribution of the incident beam is that given in Figure 3. According to the experimental conditions described in Section 2, electrons scattered are not deflected due to the intense magnetic field but they do lose energy in the forward (if the hypothetical scattering angle is less than 90 degrees) or backward (if it is higher than 90 degrees) directions. Note that the consequence of a 90 degree elastic or inelastic collision is that the electron stops completely. Back-scattered

Table 2. Present experimental results of total electron scattering cross sections for furfural.

Energy (eV)	Total cross section ($\times 10^{-20}$ m^2)	Statistical uncertainty (%)	$\pm$ Total uncertainty limit ($\times 10^{-20}$ m^2)	Missing angles (deg.)
7	50.7	6.3	3.5	0–13, 167–180
10	43.2	4.9	2.6	0–10, 170–180
20	44.0	6.4	3.1	0–7, 173–180

Fig. 8. The energy distribution of 10 eV electrons transmitted through the retarding field analyser, when the gas cell contains 1 mTorr of furfural.

electrons are returned to the chamber with their own kinetic energy once they come under the influence of the repulsive field close to the cathode. Furthermore, inelastic excitations imply additional energy loss which makes more complicated the energy profiles of the transmitted electrons.

From Figure 8, there is excellent agreement between the electron transport simulation and the experiment for energies from 10 eV down to about 4 eV. Below this energy, however, the simulation is much more effective in stopping the electrons (i.e. relatively less electrons are transmitted) than the experimental observation. Although our simulation uses the IAM-SCAR+I calculated cross sections, and this method is not so accurate at such low energies [1], the effect is so dramatic that we should also consider an instrumental effect to explain in part the discrepancy observed in Figure 8. For example, when simulating the electron transport we assume a uniform axial magnetic field along the gas cell but, in practice, the magnetic field is not completely uniform over 1–2 cm from the ends of the scattering chamber. Reproducing those variations in the field in these regions is non-trivial, with the present configuration of our Monte Carlo code, but a further improvement in the experimental setup, by implementing a new scattering cell inside the magnetic coil chamber, which is at least 4 cm shorter than it is now, might be a technical improvement of further study.

Despite the limitations, the Monte Carlo simulation provides valuable information that can be used to improve

experimental procedures in order to obtain more accurate TCS data. For example, as shown in Table 3 the transport simulation gives information about the number and type of scattering events taking place in the SC. This has relevance to the importance of multiple scattering processes, or the most effective position of the operating point can also be derived from this data.

It is clear from Table 3 that for the present magnetic confinement conditions, elastic scattering is the most effective process for slowing down the electron beam (note that rotational excitations are not distinguishable in our experiment with the energy resolution used). In addition, even in the low pressure regime we are considering here, Table 3 also indicates that multiple scattering due to elastic collisions could affect the TCS measurements.

The results presented in this section suggest that the experimental configuration used in this study will probably require further improvements, in order to reduce systematic errors affecting the TCS measurements and in improving the magnetic field uniformity along the gas cell but particularly near its ends.

5 Conclusions

A magnetically confined electron-beam-transmission experiment has been described and applied to measure total electron scattering cross sections for furfural, at selected incident energies of 7, 10 and 20 eV. This experimental system has also been used to determine the energy distribution of 10 eV electrons after their interaction with 1 mTorr of furfural contained in a 240 mm length gas cell. In addition, a complete set of electron scattering cross section and energy loss data, in the energy range 0–20 eV, has been assembled from previous measurements and calculations. Especially, differential and integral elastic cross sections as well as integral inelastic (electronic excitation and ionisation) cross sections, have been calculated with our latest IAM-SCAR+I method [1]. Vibrational excitation cross sections and the energy loss distribution functions were taken from our previous measurements [3]. For completeness, rotational excitation was calculated with a Born type method [1]. This collisional set of data was subsequently used as input parameters for an event-by-event Monte Carlo simulation procedure to model the electron transport along the gas cell. The simulated energy distribution of the transmitted electrons was found to be in good agreement with the experimental observation for electron energies between 4 and 10 eV. Discrepancies below this energy suggested that either experimental conditions need to be modified in order to reduce remaining systematic errors, or there were limitations with the lower

Table 3. The number and type of interactions occurring for 10^7 incident electrons with 10 eV energy colliding with 1 mTorr of furfural in the scattering chamber. Energy deposition and multiple collision data are also shown.

Type of interaction	Number of interactions	Energy deposition (eV)	Number of collisions per primary electron
Elastic	6.6×10^7	6.2×10^7	6.6
Electronic excitation	6.1×10^4	4.4×10^5	0.061
Vibrational excitation	−		
Ionisation	295	2.8×10^3	3×10^{-5}
Rotational excitation	4.2×10^8	4.6×10^5	42

energy IAM-SCAR+I cross sections used in the modelling. We simulated here a relatively simple experiment in very specific conditions. A future swarm experiment in furfural would be desirable in order to check the consistency of the cross sections in a broader context.

Author contribution statement

A.I. Lozano: total cross section measurements and data analysis; K. Krupa: experimental arrangement; F. Ferreira da Silva: data analysis and result discussion; P. Limão-Vieira: experimental design; F. Blanco: electron scattering calculation; A. Muñoz: electron transport simulation, D.B. Jones: electron energy loss measurements; M.J. Brunger: providing additional electron scattering data; G. García: coordination and support.

References

1. D.B. Jones, R.F. da Costa, M.T. do N. Varella, M.H.F. Bettega, M.A.P. Lima, F. Blanco, G. García, M.J. Brunger, J. Chem. Phys. **144**, 144303 (2016)
2. R. Costa, M.T. do N. Varella, M.H.F. Bettega, R.F.C. Neves, M.C.A. Lopes, F. Blanco, G. García, D.B. Jones, M.J. Brunger, M.A.P. Lima, J. Chem. Phys. **144**, 124310 (2016)
3. D.B. Jones, R.F.C. Neves, M.C.A. Lopes, R.F. da Costa, M.T. do N. Varella, M.H.F. Bettega, M.A.P. Lima, G. García, F. Blanco, M.J. Brunger, J. Chem. Phys. **143**, 224304 (2015)
4. D.B. Jones, R.F.C. Neves, M.C.A. Lopes, R.F. da Costa, M.T. do N. Varella, M.H.F. Bettega, M.A.P. Lima, G. García, P. Limão-Vieira, M.J. Brunger, J. Chem. Phys. **144**, 124309 (2016)
5. A.S. Mamman, J.-M. Lee, Y.-C. Kim, I.T. Hwang, N.-J. Park, Y.K. Hwang, J.-S. Chang, J.-S. Hwang, Biofuels Bioprod. Biorefin. **2**, 438 (2008)
6. A.W. Khan, J.-P. Labrie, J. McKeown, Biotechnol. Bioeng. **28**, 1449 (1986)
7. J. Amorim, C. Oliveira, J.A. Souza-Corrêa, M.A. Ridenti, Plasma Process. Polym. **10**, 670 (2013)
8. M.A. Ridenti, J.A. Filho, M.J. Brunger, R.F. da Costa, M.T. do N. Varella, M.H.F. Bettega, M.A.P. Lima, Eur. Phys. J. D **70**, 161 (2016)
9. F. Ferreira da Silva, E. Lange, P. Limão-Vieira, N.C. Jones, S.V. Hoffmann, M.-J. Hubin-Fraskin, J. Delwiche, M.J. Brunger, R.F.C. Neves, M.C.A. Lopes, E.M. de Oliveira, R.F. da Costa, M.T. do N. Varella, M.H.F. Bettega, F. Blanco, G. García, M.A.P. Lima, D.B. Jones, J. Chem. Phys. **143**, 144308 (2015)
10. D.B. Jones, E. Ali, K.L. Nixon, P. Limão-Vieira, M.-J. Hubin-Franskin, J. Delwiche, C.G. Ning, J. Colgan, A.J. Murray, D.H. Madison, M.J. Brunger, J. Chem. Phys. **143**, 184310 (2015)
11. A. Traoré Dubuis, A. Verkhovtsev, L. Ellis-Gibbins, K. Krupa, F. Blanco, M.A.P. Lima, D.J. Jones, M.J. Brunger, G. García, J. Chem. Phys. (2017) in press
12. M.C. Fuss, A.G. Sanz, F. Blanco, J.C. Oller, P. Limão-Vieira, M.J. Brunger, G. García, Phys. Rev. A **88**, 042702 (2013)
13. A.G. Sanz, M.C. Fuss, F. Blanco, J.D. Gorfinkiel, D. Almeida, F. Ferreira da Silva, P. Limão-Vieira, M.J. Brunger, G. García, J. Chem. Phys. **139**, 184310 (2013)
14. Y. Itikawa, J. Phys. Chem. Ref. Data **35**, 31 (2006)
15. F. Blanco, A. Muñoz, D. Almeida, F. Ferreira da Silva, P. Limão-Vieira, M.C. Fuss, A.G. Sanz, G. García, Eur. Phys. J. D **67**, 199 (2013)
16. F. Blanco, L. Ellis-Gibbings, G. García, Chem. Phys. Lett. **645**, 71 (2016)